Germline deletion of *Cetn1* causes infertility in male mice

Prachee Avasthi[1,*,#], Jan Frederik Scheel[2,*], Guoxin Ying[1], Jeanne M. Frederick[1], Wolfgang Baehr[1,3,4], Uwe Wolfrum[2]

Supplemental figures and tables

Figure S1.

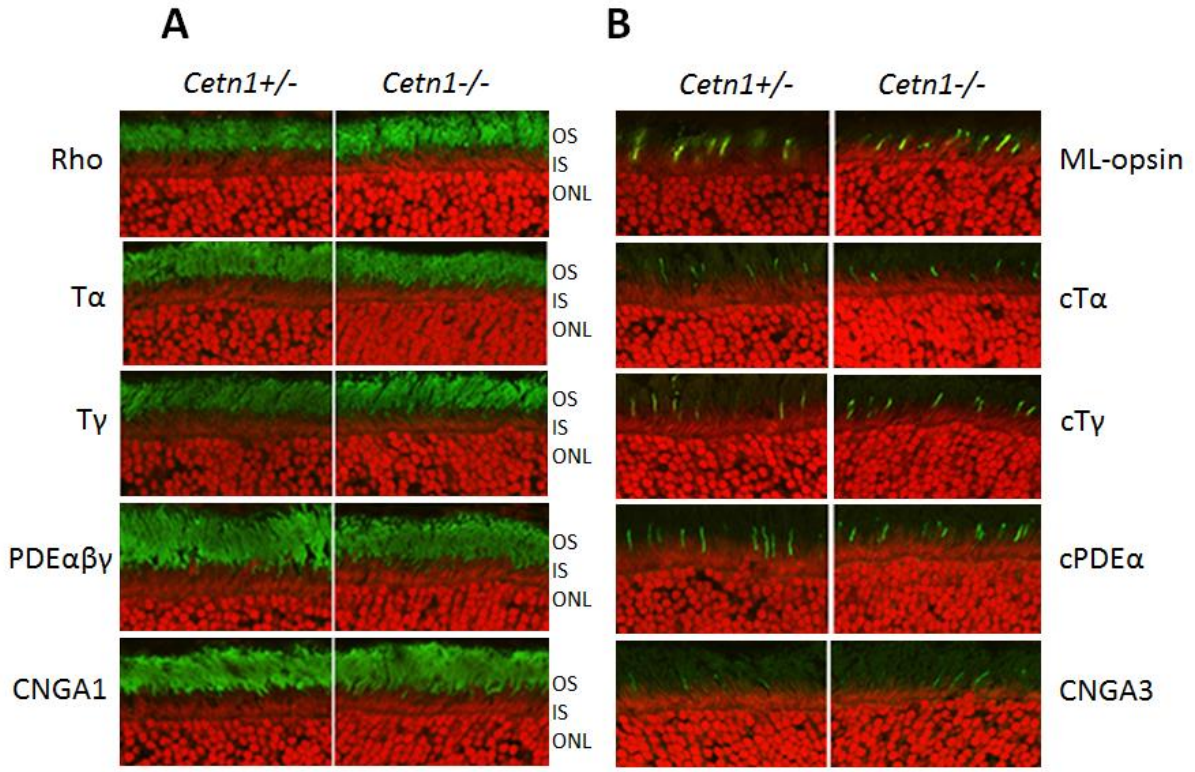

Figure S1. Immunolocalization of phototransduction proteins in retinas of *Cetn1*$^{+/-}$ and *Cetn1*$^{-/-}$ mice. **A** (left vertical panel), localization of rhodopsin, transducin subunits, PDEαβγ, and CNGA1 in rod outer segments. **B** (right vertical panel), distribution of ML-opsin, cone transducin (cTα), cone PDEα, and CNGA3 in cone outer segments. Heterozygote retinas, indistinguishable from wild-type, were used as reference. Sections of heterozygote (left) and homozygous knockout (right) retinas were immunolabeled using antibodies directed against the indicated target antigens (green) and contrasted with propidium iodide (red). Antibodies used to detect rod- and cone-specific antigens have been described (Avasthi et al., 2009; Baehr et al., 2007; Zhang et al., 2008). No obvious difference in localizations was observed between genotypes. OS, outer segments; IS, inner segments; ONL, outer nuclear layer.

Figure S2.

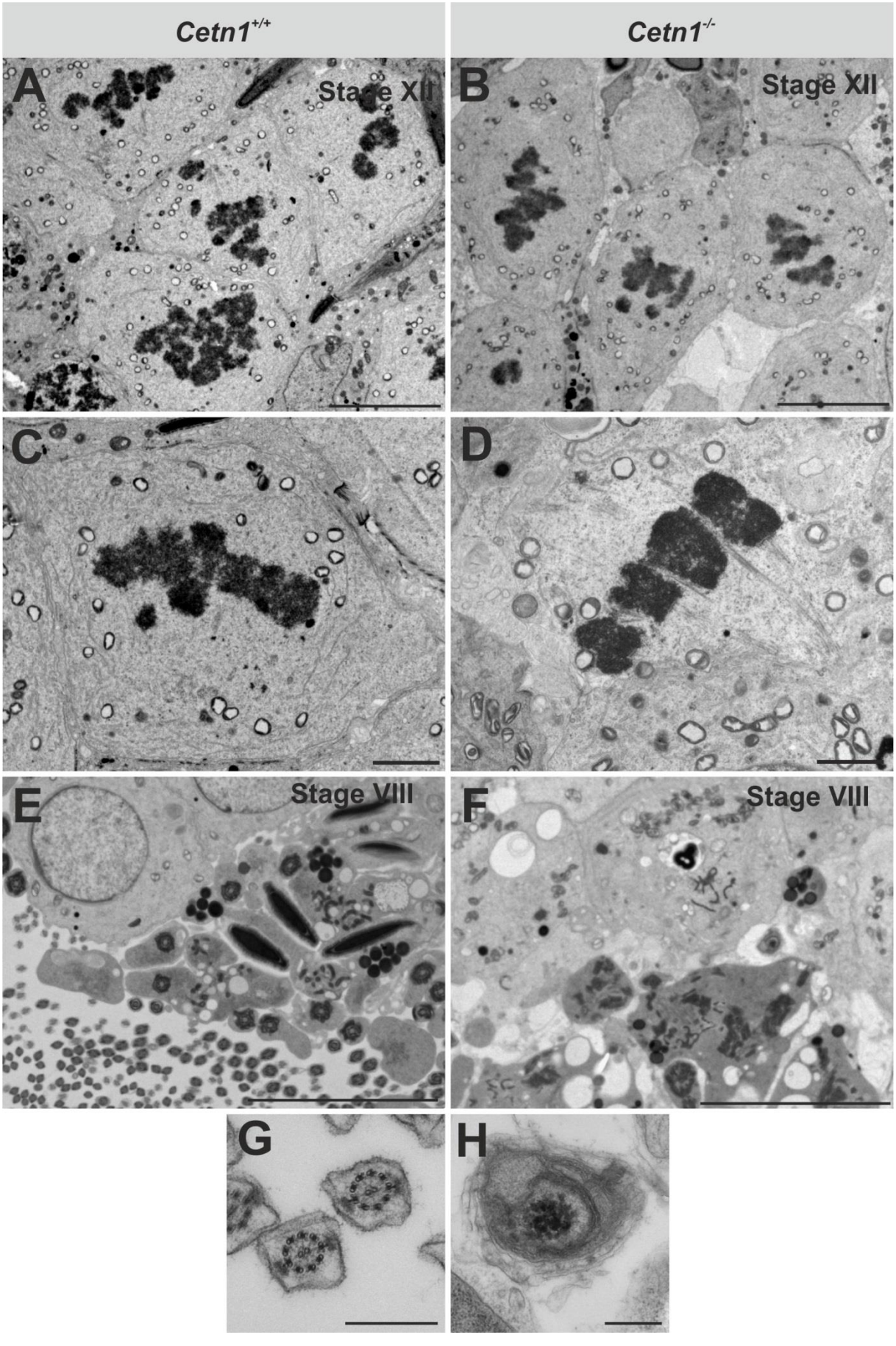
Cetn1+/+
Cetn1-/-
A
Stage XII
B
Stage XII
C
D
E
Stage VIII
F
Stage VIII
G
H

Figure S2. Electron microscope analysis of seminifereous tubules of Cetn1$^{+/+}$ and Cetn1$^{-/-}$ mice. A, B spermatocytes during meiosis of stage XII seminiferous tubules. Normal condensation and chromosome pairing is evident in spermatocytes of *Cetn1*$^{-/-}$ seminiferous tubules. **C, D** higher magnifications of spermatocytes in metaphase. Chromosomes are equatorially arranged in Cetn1$^{+/+}$ and Cetn1$^{-/-}$. The arrangement of spindle microtubules in *Cetn1*$^{-/-}$ appeared normal. **E, F** 2nd generation spermatids directly prior to spermiation at stage VIII in *Cetn1*$^{+/+}$ and *Cetn1*$^{-/-}$ seminiferous tubules. In E, elongated and mature spermatid heads are found facing the tubule lumen and additionally, several spermatid flagella are observed in cross section. In F, electron-dense material is present instead of mature spermatids. **G,** cross section through a *Cetn1*$^{+/+}$ flagellum showing the characteristic axonemal microtubule 9x2+2 arrangement and side fibers. **H,** cross section through the sole *Cetn1*$^{-/-}$ flagellum found, revealing severe disorganization of axonemal microtubules. **Bars: A, B, E, F: 5 µm, C, D: 1 µm, G, H: 0.5 µm.**

Figure S3.

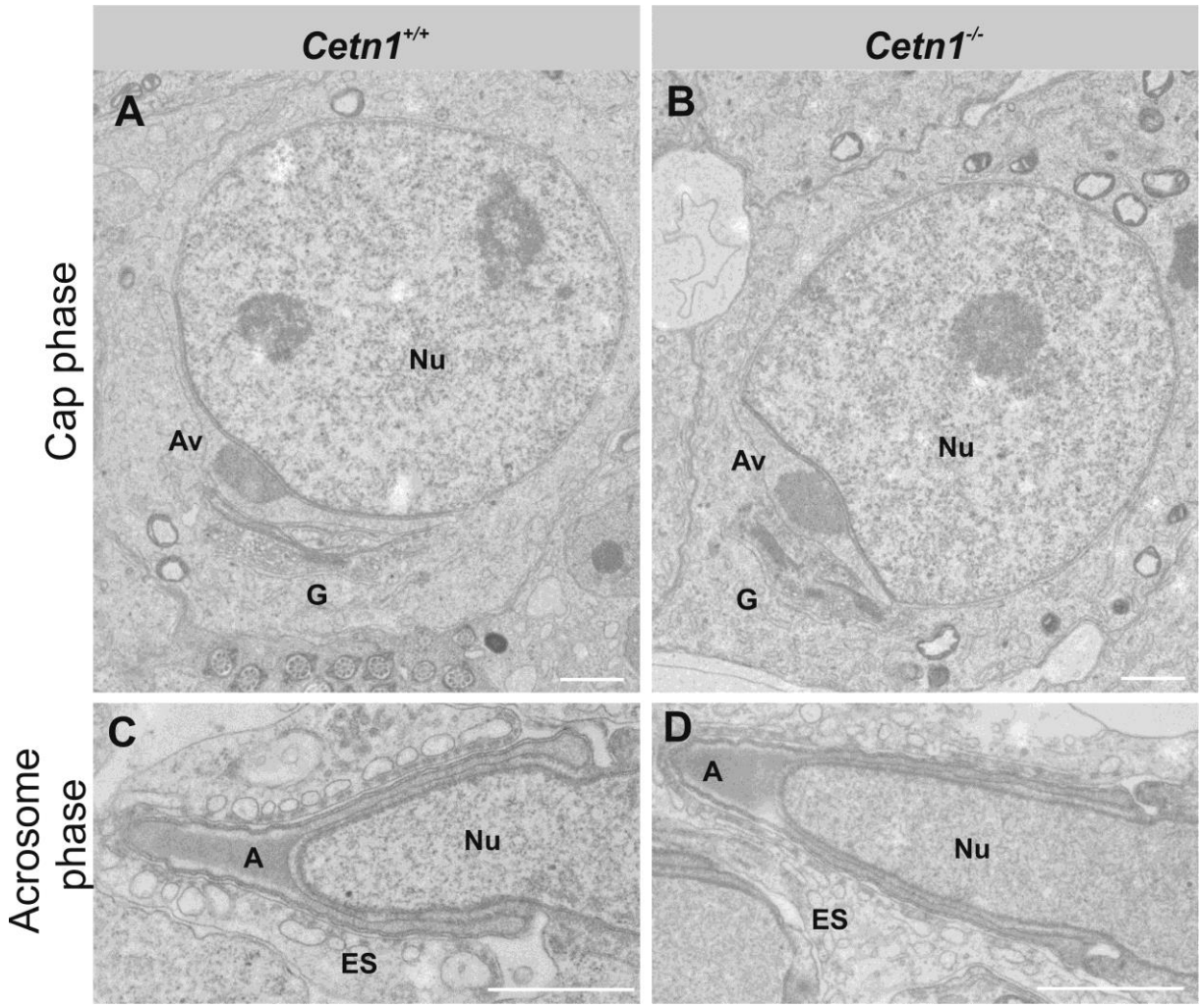

Figure S3. Transmission electron micrographs of early-stage spermiogenesis from *Cetn1*$^{+/+}$ and *Cetn1*$^{-/-}$ mice. A, B cap phase spermatids from *Cetn1*$^{+/+}$ and *Cetn1*$^{-/-}$ mice, and **C, D** acrosome phase spermatids display no difference in ultrastructure. **Av:** acrosomic vesicle, **G:** Golgi apparatus, **Nu:** nucleus, **A:** acrosome, **ES:** ectoplasmic specialization. **Bars: 1 µm.**

Figure S4.

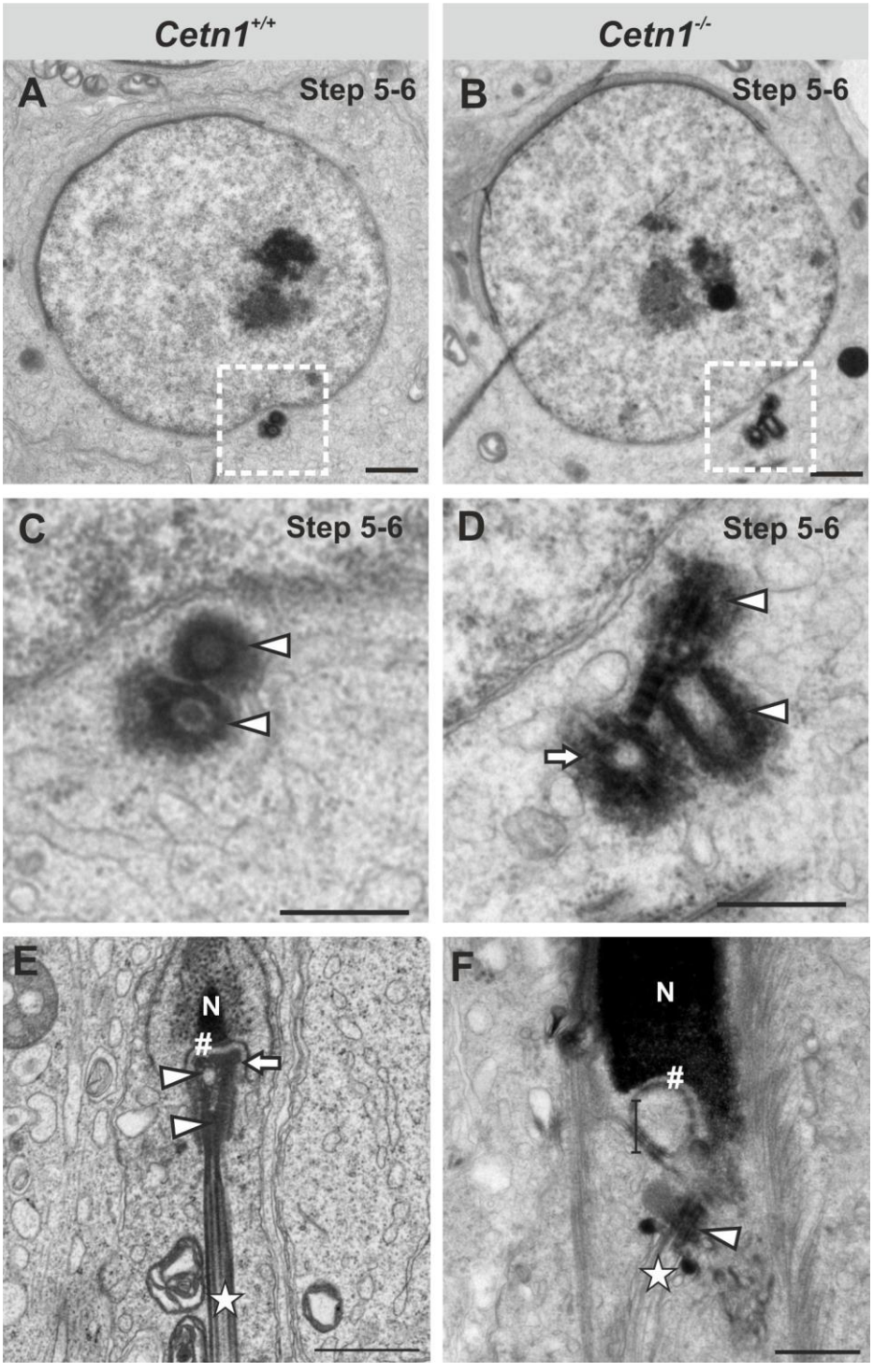

Figure S4. Electron microscopy of spermatid centrioles. **A, B,** round post-meiotic spermatids in step 5-6 of *Cetn1*$^{+/+}$ and *Cetn1*$^{-/-}$ testes. Centrioles of the centrosome/basal body complex are located within the perinuclear compartment. **C, D,** higher magnification taken from A and B. No abnormalities were detectable in *Cetn1*$^{-/-}$ spermatid centrioles (**arrowheads**); adjunct (**arrow**) formation was initiated and centriole sizes were of normal proportions (see text). **E,F,** mature spermatids in step 15. **E,** fully-developed striated body (**arrowhead**) of a *Cetn1*$^{+/+}$ mouse spermatid embedded in the nuclear fossa (**#**) of the nucleus (**N**). The sperm flagella axoneme (**star**) exhibited a dense structure with straight projection from the striated body. **F,** The centriolar complex (**arrowhead**), observed rarely in mature *Cetn1*$^{-/-}$ spermatids, lacks a striated body. The axoneme (**star**), nuclear fossa (**#**) and basal body (**arrowhead**) each exhibit unstable, atypical structure. **Bars: A, B: 1 µm, C - F: 0.5 µm.**

Figure S5.

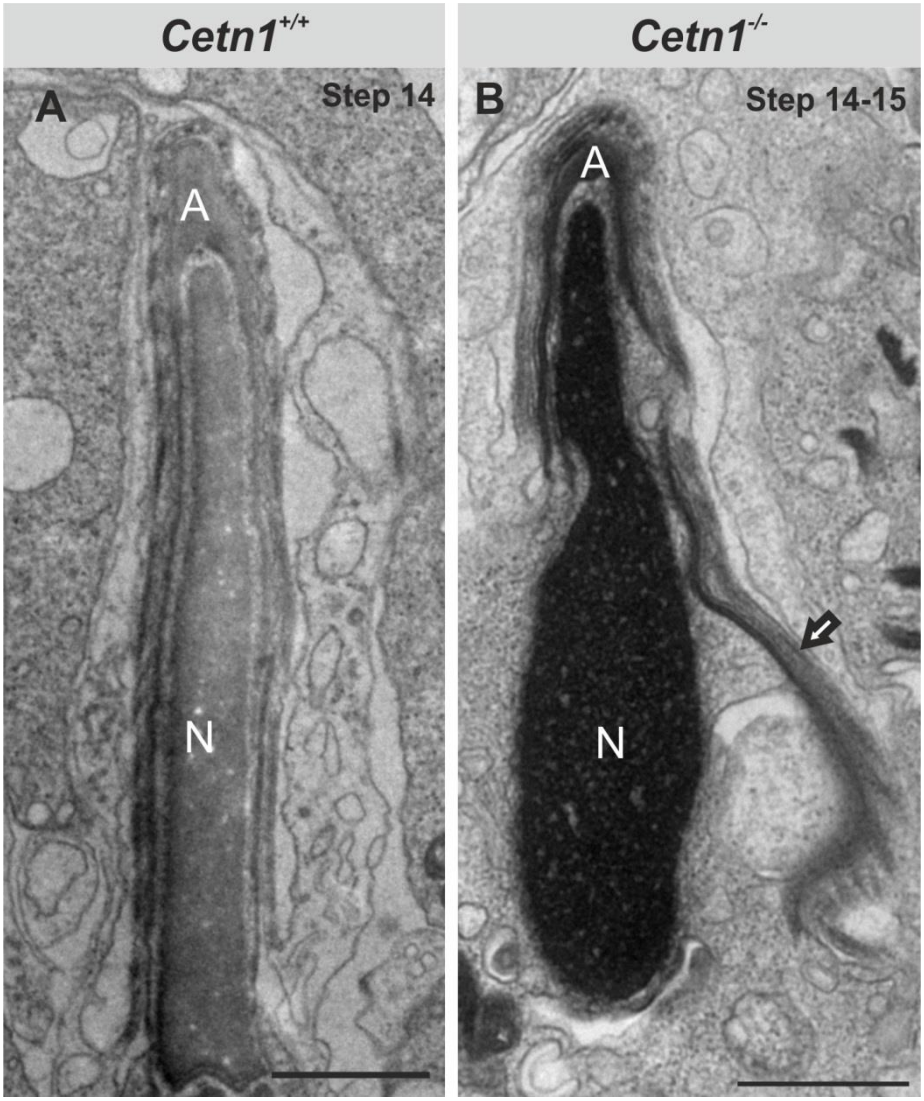

Figure S5. Ultrastructure of step 14-15 spermatids. A, *Cetn1*$^{+/+}$ spermatid at step 14 with normal acrosome **(A)** and nucleus **(N)** morphology. **B**, *Cetn1*$^{-/-}$ spermatid at step 14-15 displays severe defects in membrane systems. The acrosome **(A)** disintegrates and dissolves **(arrow)** from the electron-dense spermatid nucleus **(N)**. **Bars: 0.5 µm.**

Figure S6.

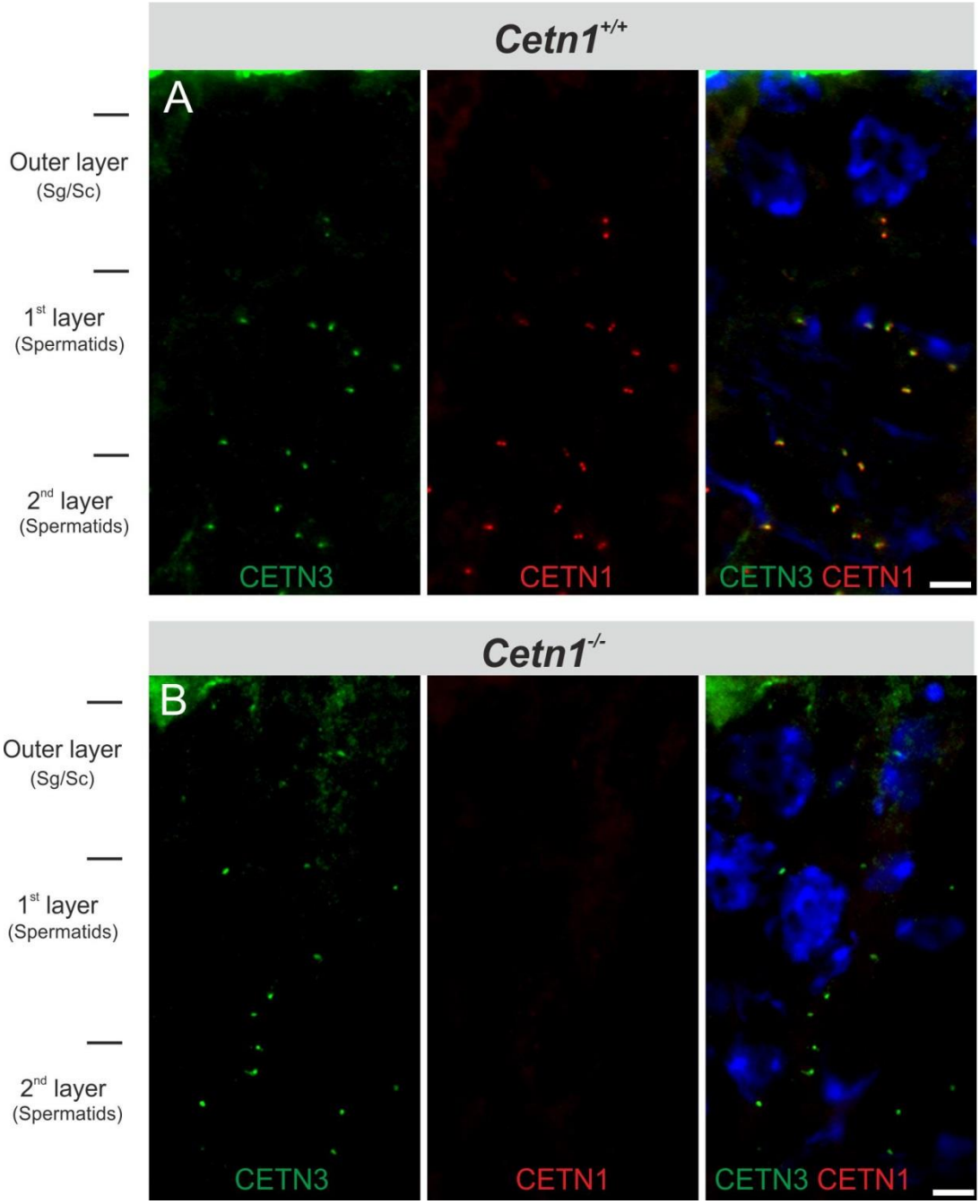

Figure S6. CETN1 and CETN3 immunolabeling of seminifereous tubules from *Cetn1*$^{+/+}$ and *Cetn1*$^{-/-}$ mice. A Antibodies directed against CETN1 (red) and CETN3 (green) label centrioles (fluorescent dots) in all layers and germ cell types of *Cetn1*$^{+/+}$ seminifereous tubules. **B** CETN3 labeling was present in all germ cell types, while CETN1 was undetectable in *Cetn1*$^{-/-}$ mice. DAPI (blue) staining of nuclei. **Sg:** spermatogonia; **Sc:** spermatocytes. **Bars: 5 µm.**

Figure S7.

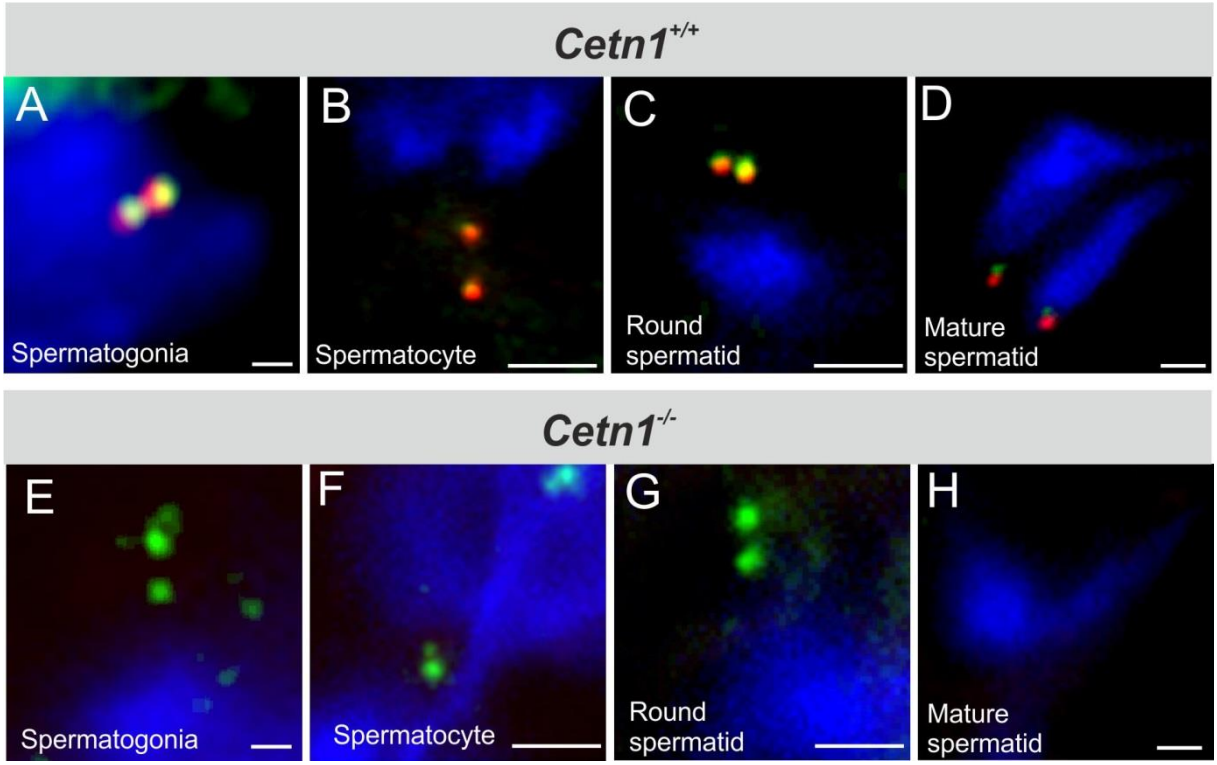

Figure S7. CETN1 (red) and CETN3 (green) immunolabeling of spermatogonia (A, E), spermatocytes (B, F), round spermatids (C, G) and mature spermatids (D, I) of seminifereous tubules from *Cetn1*$^{+/+}$ and *Cetn1*$^{-/-}$ mice. No obvious difference of CETN3 labeling was discerned between *Cetn1*$^{+/+}$ and *Cetn1*$^{-/-}$ spermatogonia, spermatocytes and early round spermatids. By contrast, sperm heads (DAPI, blue) of *Cetn1*$^{-/-}$ mature spermatids (**H**) were "bent" with centrioles displaying no immunoreactivity for CETN3 as well as CETN1. **Bars: 1 µm**.

Supplemental Table

Table S1: *Cetn1* mice body weights, testis weights, sperm number and deformed sperm among genotypes.

Genotype	Body weight (g)	Testis weight (mg)	Amount of sperm (%)	% sperm deformed
***Cetn1*$^{+/+}$**	31.6 ±2.5	93 ±6	100%	1.5% ±0.2
***Cetn1*$^{+/-}$**	30.9 ±2.7	92 ±3	100% ±1.8	1.7% ±0.4
***Cetn1*$^{-/-}$**	32.1 ±2.1	94 ±4	1.1% ±0.2	100%

Male mice from 6 litters were analyzed (N=24, consisting of five *Cetn1*$^{+/+}$, eleven *Cetn1*$^{+/-}$ and eight *Cetn1*$^{-/-}$). No abnormality of body or testis weight was measurable. Average total sperm count of *Cetn1*$^{+/+}$ mice was set to 100%; no difference in *Cetn1*$^{+/-}$ sperm count was found. *Cetn1*$^{-/-}$ sperm number was reduced drastically to 1.1% ±0.2, with 100% of these exhibiting deformation.

Table S2: Quantification of the number of germ cell types in seminifereous tubuli of Cetn $^{+/+}$ and Cetn1$^{-/-}$ mice.

Genotype	No. spermatogonia	No. spermatocytes	No. spermatids	Epithelial thickness (µm)
***Cetn1*$^{+/+}$**	3.0 ±1.4	4.4 ±1.1	16.2 ±6.8	92.1 ±3.2
***Cetn1*$^{-/-}$**	3.2 ±0.8	3.8 ±1.2	16.8 ±5.0	91.0 ±3.2

Quantification of the numbers of germ cell types from *Cetn1*$^{+/+}$ and *Cetn1*$^{-/-}$ seminifereous tubuli (N=5). Germ cells of *Cetn1*$^{+/+}$ and *Cetn1*$^{-/-}$ tubuli seminiferi at stage IX of spermatogenesis were counted in the area of a rectangle 100 µm x 50 µm. No significant difference in average values was detected for *Cetn1*$^{-/-}$ germ cells.